Microarcs as a Termination Mechanism of Optical Pulses in Electric-Discharge-Excited KrF Excimer Lasers

Mark J. Kushner, *Fellow, IEEE*

Abstract—**The optical pulse in electric-discharge-excited excimer lasers often terminates prior to the end of the current pulse. This behavior has been attributed to the formation of filamentary microarcs in the discharge volume. In this paper, we theoretically investigate both macroscopic (≥ mm's to cm's) and microscopic (< 100's μm) nonuniformities in electric field, preionization density, and halogen density as precursors to arcs and microarcs in KrF lasers. Macroscopic nonuniformities lead to volumetric arcing. Microscopic nonuniformities lead to filamentary arcs and streamers. We find that microarcs may terminate the optical pulse due to disruption of the optical homogeneity of the plasma prior to the collapse of impedance of the discharge. Small-scale microscopic inhomogeneities (< 10's–100 μm) develop into microarcs sooner than large-scale homogeneities (> 10's–100 μm) due to the higher pressure gradient afforded by their small size. Large-scale inhomogeneities, though, are ultimately more detrimental to the performance of the laser.**

I. Introduction

ELECTRICAL-discharge excimer lasers (XeCl [308 nm], KrF [248 nm], ArF [192 nm]) are practical devices for delivering high peak and high average optical power in the ultraviolet [1]–[5]. Single-pulse energies exceeding 60 J at from the XeCl($B \rightarrow X$) transition [6], [7], repetition rates exceeding 1 kHz [8] and efficiencies > 4% [9] have been obtained with research devices. The rapidly improving technology of these devices is demonstrated by the fact that high repetition-rate excimer lasers, operating with average powers of 100–200 W ($\simeq$ 1 J/pulse at a few hundred Hz), are now commercially available [10]. In spite of these impressive specifications, the optical pulse lengths of typical electric-discharge excimer lasers are still only 10's of ns [8], [10], although pulse lengths of 100's ns [9], [11] to 1.5 μs [12] have been obtained in single-pulse research devices. The termination mechanism for laser action in short (10's ns) optical pulse lasers, which operate in an avalanche mode, is usually discharge constriction or arcing [13], [14]. Long (100's ns) optical pulse lasers usually operate in a quasi-cw mode with current fed from a pulse forming line (PFL) [9], [11], [12], [15]. The termination mechanism in these devices is qualitatively different than that for the short pulse devices. Small arcs or microstreamers develop in the discharge of long pulse devices which "consume" the uniform glow and eventually terminate the laser pulse [15]. The impedance of the discharge, though, remains high and volume-averaged power deposition continues.

In this paper we investigate the formation of microarcs as a termination mechanism of optical pulses in electric-discharge-excited KrF excimer lasers. The study is performed by modeling the electron kinetics and plasma chemistry of both the bulk plasma and in the vicinity of a microarc. The latter portion of the model includes integrating the hydrodynamic equations of motion. We find that there are two spatial scales over which nonuniformities can terminate the optical pulse of an excimer laser: The larger scale (> mm's) results in constriction of the discharge and arcing. The optical pulse terminates due to impedance collapse of the discharge or depletion of the halogen donor. The smaller scale (< 10's–100's μm) results in microarcs which terminate the optical pulse prior to impedance collapse by disrupting the optical homogeneity of the discharge. At that time, power is still being deposited in the bulk plasma.

In Section II, considerations for obtaining long optical pulses in excimer lasers are discussed, and experimental observations of microarcs in electric-discharge excimer lasers are reviewed. The model used in our study is described in Section III, followed by a discussion of our results in Section IV. Our concluding remarks are in Section V.

II. Considerations for Obtaining Long Optical Pulses

The gas mixtures used in electric-discharge excimer lasers are typically composed of a large mole fraction of a rare gas buffer, and small mole fractions of the excimer producing species (another rare gas and a halogen donor). For example, a KrF discharge-excited laser may have a $He/Kr/F_2 = 99/1/0.1$ mixture at a total pressure of 1–5 atm. With the exception of the halogen donor, which usually has only a small mole fraction (< 0.5%), the lowest excited electronic state in the plasma is the upper laser level (e.g., XeCl(B, C), KrF(B)). Therefore energy deposited in the plasma naturally flows to the upper laser level by a series of excitation transfer reactions [16]. For example, after the initial electron-impact ionization reaction in a KrF($B \rightarrow X$) laser, one possible flow of energy resulting in excitation of the upper laser level is:

$$\begin{array}{lccccc} \text{Reaction}: & e + \text{He} \rightarrow \text{He}^+ & \overset{2\text{He}}{\rightarrow} & \text{He}_2^+ & \overset{\text{Kr}}{\rightarrow} & \text{Kr}^+ \overset{\text{Kr+He}}{\rightarrow} \\ \text{Energy (eV)}: & 24.6 & & 22.2 & & 14.0 \\ & \text{Kr}_2^+ & \overset{e}{\rightarrow} & \text{Kr}(5s) & \overset{F_2}{\rightarrow} & \text{KrF(B)}. \\ & 12.8 & & 9.7 & & 5.0 \end{array} \quad (1)$$

As a result of this flow of energy to the upper laser level the formation efficiency of that state can be quite large (20% in the example). Formation of the upper laser level is, therefore, not typically constrained by competing kinetic chains. Under these conditions, the rate of formation of the upper laser level is largely a function of power deposition. Once the upper laser level is formed, however, other processes may reduce laser power. These processes include quenching by electrons, the halogen donor, and

Manuscript received June 29, 1990; revised November 1, 1990. This work was supported by the Sandia National Laboratories, the Los Alamos National Laboratory, and the National Science Foundation under Contract Nos. ECS88-15781 and CBT88-03170.

The author is with the Department of Electrical and Computer Engineering, University of Illinois, 1406 W. Green Street, Urbana, IL 61801.

IEEE Log Number 9042736.

0093–3813/91/0400–0387$01.00 © 1991 IEEE

the more massive rare gases, and absorption of the laser radiation by plasma species. Nevertheless, the local power deposition and kinetic formation efficiency set an upper limit on the maximum extractable laser power. Therefore uniformly depositing power for the longest possible time is one of the greatest concerns in constructing an electric-discharge excimer laser [5], [14], [15], [17]–[20].

The optical pulse lengths of electric-discharge lasers are generally only 10's ns long. In most devices, the optical pulse is terminated by arcing or instabilities in the discharge, as opposed to any particular kinetic process. These instabilities are initiated by some nonuniformity in power deposition. The uniformity of power deposition during the current pulse in an excimer laser is largely determined by the distribution of the preionization density and of the uniformity of the electric field provided by the electrode profiles. Following this argument, great care has been expended in making these distributions as uniform as possible in order to extend the pulse length by reducing the propensity towards arcing or generating discharge instabilities. Using spark arrays [12], X-ray [21], [22], corona preionization [23], and spiker-sustainer discharge circuits [9], [11], [15], pulse lengths of 400 ns–1.5 μs have been obtained with XeCl [15], and 200 ns–800 ns in KrF [3].

The acute requirement to uniformly preionize and excite excimer laser discharges results from the fact that ionization is largely balanced by attachment, and also the fact that the attaching species is usually consumed during the discharge pulse. In excimer laser discharges, electron loss by diffusion is negligible, and recombination of dimer ions is a minor loss mechanism under optimum conditions. Under quasi-steady-state conditions, the local self-sustaining electric field is therefore set by that value which results in a balance between electron-impact ionization and electron loss by attachment to the halogen donor. The quasi-steady-state operating point of the discharge at any particular spatial location $\vec{r}$ is that value which satisfies:

$$\sum_j f_j(\vec{r}) \cdot k_{I_j}(E/N(\vec{r})) = \sum_j f_j(\vec{r}) \cdot k_{a_j}(E/N(\vec{r})) \qquad (2)$$

where f_j is the mole fraction of the component j; k_{I_j} is its ionization rate coefficient; k_{a_j} is its attachment rate coefficient; and E/N is the electric field normalized by the gas density. In writing (2), we have used the Local Field Approximation (LFA), which states that the electron-energy distribution can be characterized by the local instantaneous value of E/N, a condition which applies during the quasi-cw portion of the current pulse [20]. The operating point of the discharge can therefore be obtained from the intersection of the mole fraction-weighted values of the ionization and attachment coefficients $\bar{k}_I$ and $\bar{k}_a$, as shown in Fig. 1. For typical lasers, the self-sustaining value of the electric field is $(E/N)_s \approx 2$–5 Td (1 Td $= 1 \times 10^{-17}$ V–cm^{-2}) [4], [9] or $(E/p)_s \approx 0.4$–1.0 kV/cm–atm.

The rate coefficients for ionization and attachment are functions of the gas mixture (e.g., halogen density), excited-state density, and electron density, in addition to being functions of E/N. Therefore the operating point in a discharge may vary as a function of position as these parameters vary as a function of position. An operating point instability (OPI) may occur when the operating point of the discharge, that is, the E/N which satisfies (2), is different as a function of position, while the discharge cannot operate at all of those points simultaneously.

The OPI is most important when discharge conditions vary transversely to the applied field [24]. In this case the device can be well represented by a network of parallel resistors, or

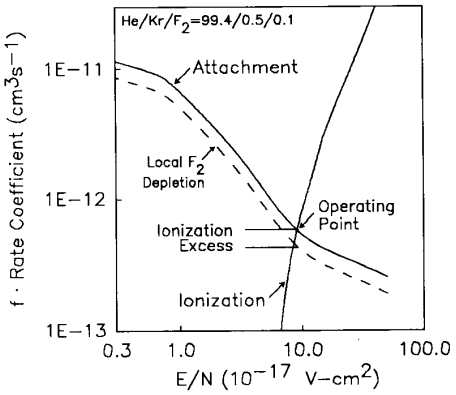

Fig. 1. Mole-fraction-weighted electron-impact rate coefficients for ionization and attachment in a He/Kr/F_2 mixture. The operating point is at the intersection of the ionization and attachment curves. An ionization excess results from local depletion of F_2, which reduces the local operating point below the discharge-averaged value of E/N.

plasma segments, in which the E/N is the same for each plasma segment. If, for example, the halogen density varies as a function of transverse position, causing $(E/N)_s$ to also vary, then it is not possible to simultaneously be at the operating point of every spatial position in the discharge (see Fig. 1). Since $(E/N)_s$ is highest where the halogen density is the largest, then there will be an ionization excess at locations where the halogen density is lower. An ionization excess is defined as occurring in segments where $\bar{k}_I(E/N) > \bar{k}_a(E/N)$. The electron density therefore increases in those plasma segments. If the halogen donor is consumed by the attachment process (e.g., $e + F_2 \rightarrow F^- + F$) and not replenished during the discharge pulse, then the rate of consumption of the halogen also increases in these segments, resulting in a lower $(E/N)_s$ and higher ionization excess. This process leads to a higher electron density and further burnup. The process is unstable and will eventually lead to arcing.

So to maximize the efficiency and lengthen the optical pulse of an electric discharge excimer laser, one must uniformly excite the gas and insure that the operating point of all spatial locations is the same. This is accomplished, in part, by having a uniform preionization and halogen density. There are two spatial scales, though, on which one must maintain this uniformity: The macroscopic (mm's to cm's), and microscopic (< 10's–100's μm). For example, electric field distributions or preionization densities which are nonuniform over macroscopic dimensions can lead to constriction of the discharge and eventual arcing, as described above. Preionization densities which are uniform over macroscopic dimensions, but not uniform over microscopic dimensions, can result in a filamentary discharge which, although it appears to the eye to be a glow in character, is not optimum for exciting a laser.

One measure of uniformity is given by the absolute value of the preionization density. In this vein, Levatter and Lin modeled the early stages of development of high-pressure preionized pulsed gas discharges [25]. They hypothesized that each individual preionization electron forms the seed of a microstreamer. As avalanche proceeds, the head of the streamer expands by diffusion. If during the formative stage of the discharge (that is, during avalanche) the transverse diffusion of the head of each streamer overlaps its neighboring streamers, then Levatter and Lin predicted that the discharge will develop as a uniform

glow. If, however, the heads of the microstreamers do not overlap, the discharge will be filamentary in character, with power primarily being deposited in small, randomly placed channels. This method of power deposition is obviously not optimum for laser applications where the laser flux should see a uniformly distributed gain. Using Levatter and Lin's criterion, microscopically uniform excimer laser discharges can only be obtained if the initial preionization electron density n_{e0} is:

$$n_{e0}(\mathrm{cm}^{-3}) > \frac{5 \times 10^6}{t_0^{2/3}(\mathrm{ns})} p^{3/2}(\mathrm{atm}) \tag{3}$$

where t_0 is the voltage rise time (ns), and p is the gas pressure (atm). For typical discharges (t_0 = 10's of ns, p = 2–4 atm), one must have $n_{e0} \gg 2 \times 10^6$ cm^{-6}. This is a value which is easily obtained in excimer laser discharges using corona and X-ray preionization [21], [22].

In spite of the fact that excimer laser discharges can be preionized over macroscopic dimensions to values exceeding the criterion of Lin and Levatter, these discharges still terminate in small arcs or streamers. Recent observations of the structure of XeCl excimer laser discharges by Taylor have shed considerable light on this topic [15]. Taylor took framing camera photographs of the discharge simultaneously to recording the laser intensity, voltage, and current waveforms. He found that the discharge was initially a uniform glow, but that during the discharge, streamers appeared to originate from each electrode and slowly propagate towards the center of the discharge, "consuming" the glow. Eventually, the streamers bridged the inter-electrode gap at which time laser oscillation ceased. The discharge impedence, however, did not significantly collapse as one would expect during arcing. This latter behavior indicated that power was still being deposited in the discharge, albeit possibly in an array of small arcs or streamers, in a fashion not conducive to sustaining laser oscillation.

Given that the streamers begin near the electrodes, one might assume that their origin lies with a nonuniformity associated with the electrode surface or cathode/anode sheaths. The nonuniformity then perturbs the delicate balance between electron ionization and attachment, thereby setting off a local OPI. This interpretation qualitatively agrees with the theories of Coutts and Webb [26] and Coutts [27], who hypothesized that the termination of laser oscillation in XeCl lasers results from what they call a "halogen depletion instability" (HDI), which is analogous to an OPI. The HDI is a consequence of there being local perturbations in the electron or halogen density which cause a decrease in the local halogen density due to excessive burnup. The spatial scale over which the HDI occurs is unspecified, but is described as being filamentary. The time to the onset of the HDI is predicted to scale inversely with $k_a(n_{e0}f_a)^{1/2}$. This implies that the departure from the operating point is more rapid as the absolute rate of halogen depletion increases, as opposed to the relative rate.

To investigate these issues, Osborne and Hutchinson measured the homogeneity of an XeCl excimer laser discharge by passing a dye laser beam through the discharge and observing its diffraction pattern [28]. They found that the probe beam experienced considerable scattering coincident with the termination of the laser output pulse. The volume-averaged spontaneous emission from the laser transition, though, did not decrease. These observations imply that the optical homogeneity of the discharge had been spoiled, thereby terminating the laser pulse, while power deposition continued. The fact that streamers could not be identified in framing camera photographs of the discharge led to the conclusion that the discharge had developed a dense framework of filaments whose dimensions were < 10's μm.

Given that an OPI has occurred, nonuniform gas heating will also occur which can result in advection driven by the resulting pressure gradient. Obviously, changes in gas density caused by advection can exacerbate an OPI by forcing the local value of E/N away from the required operating point. It is instructive to examine the spatial scale length and characteristic time over which changes in gas density may occur due to advection, because it is these spatial and time scales over which microarcs may develop. These scales can be estimated in the following fashion: Assume that power deposition is nonuniform to a degree α over a scale length ℓ. After a time τ the change in gas temperature is $\Delta T = \alpha P\tau/(3/2\ Nk)$ and the pressure gradient is $\nabla \boldsymbol{P} \approx (2\ \alpha P\tau)/\ell$. As this is the time rate of change of momentum density $\rho = NMv$ (M is the average molecular weight and v is the convective velocity), then $\frac{\Delta v}{\tau} \approx \nabla \boldsymbol{P}/(NM)$ and $\Delta v = 2\alpha P\tau^2/(NM\ell)$. Since $\frac{\partial N}{\partial t} = -\nabla \cdot vN$, then we can approximate:

$$\frac{\Delta N}{N} \approx \frac{2\alpha P\tau^3}{3MN\ell^2}. \tag{4}$$

For typical conditions (P = 300 kW–cm^{-3}, $\tau \approx$ 200 ns, p = 4 atm):

$$\frac{\Delta N}{N} \approx \frac{\alpha \cdot 3 \times 10^{-6}}{[\ell(\mathrm{cm})]^2}. \tag{5}$$

This scaling says that if there is nonuniformity in power deposition on the order for a few percent ($\alpha \leq 0.05$) over a distance ℓ, the gas density will remain uniform to within a few percent for a few hundred nanoseconds provided that $\ell \gg$ 10's μm. In order for the gas to remain uniform for longer pulse lengths, ℓ must be at least a few millimeters. If $\ell <$ 10's μm, then the pressure gradient is sufficiently large that advection can begin to rarify a channel, and a microarc will result within a few hundred nanoseconds. The spatial scale of small nonuniformities therefore determines whether and when a discharge will develop microarcs.

It appears, then, that for excimer laser discharges having pulse lengths less than a few microseconds and having a power deposition uniform on scale lengths of $\geq$ 0.1–1 mm, the gas remains motionless during the discharge. With this approximation, the gas-phase chemical kinetics may be considered on only a local basis, with no advection or diffusion to couple adjacent plasma segments. This is an important approximation, because it states that all spatially dependent phenomena results strictly from differences in local power deposition. We call this approximation the Stationary Kinetics Approximation (SKA). If, however, the SKA cannot be invoked, gas motion must be considered in the analysis.

III. Description of the Model

To investigate the effects of macroscopic and microscopic nonuniformities on the performance of electric-discharge-excited excimer lasers, a KrF($B \rightarrow X$) laser has been modeled. This model is a time-dependent multidimensional simulation which includes rate equations for the pertinent species, the heavy particle plasma chemistry and electron collisions, and models for the external electrical circuit and laser extraction. Electron-impact rate coefficients are obtained by solving Boltzmann's equation for the electron-energy distribution as a function of the local E/N, gas mixture, fractional ionization, and fractional excited-state density. The local electric field is obtained by requiring

current continuity and solving Laplace's equation:

$$\nabla \cdot \vec{j} = \nabla \cdot \sigma \vec{E} = -\nabla \cdot \sigma \nabla \phi = 0 \tag{6}$$

where j is the current density, σ is the local plasma conductivity, E is the electric field, and ϕ is the electric potential. Equation (6) was solved using the method of successive-over-relaxation at time intervals not exceeding 0.1 ns during the current pulse, and in most cases more frequently. The model takes two forms: The first uses the SKA and does not consider motion of the gas; the second includes convection in the manner described below. The former model is functionally the same as those previously reported and is described in detail in [9], [29]–[31].

To investigate the effect of microarcs on the performance of excimer lasers, the discharge volume was modeled as being a bulk homogeneous plasma with a random distribution of cylindrical subvolumes in which perturbations in preionization or halogen density, precursors to microarcs, occur. The perturbation and resulting microarcs were assumed to bridge the entire gap between anode and cathode (see Fig. 2). Within each subvolume, the rate equations for all plasma species were solved. In addition, the fluid-transport equations were solved for the gas density, temperature, and momentum. The form of the equations solved are:

$$\frac{\partial N}{\partial t} = -\nabla \cdot \vec{v} N + \nabla \cdot D \nabla N \tag{7}$$

$$\frac{\partial (\rho \vec{v})}{\partial t} = -\nabla p - \nabla \cdot \vec{v}(\rho \vec{v}) - \nu \vec{v} \tag{8}$$

$$\frac{\partial \left(\frac{3}{2} N k T_g\right)}{\partial t} = \vec{j} \cdot \vec{E} - \nabla \cdot \vec{v}\left(\frac{5}{2} N k T_g\right) + \nabla \cdot \kappa \nabla T_g \tag{9}$$

$$- \sum_i f_i \Delta H_i N \tag{10}$$

where N is the total gas number density, $\vec{v}$ is the advective velocity, D is the gas diffusion coefficient, ρ is total gas mass density, p is the thermodynamic pressure, T_g is the gas temperature, and ν is an effective viscous damping term. $j \cdot E$ is the local joule heating, κ is the thermal conductivity, f_i is the mole fraction of species i, and ΔH_i is the heat of formation of that species. We assumed ideal gas behavior and approximated $p = NkT_g$. Equations (7)–(9) were solved using finite differences for the spatial derivatives on a nonuniform mesh. The mesh spacing increased somewhat less than linearly with distance from the center of the microarc. The fluxes between computational cells were specified using the donor cell method. The equations were integrated in time using a third-order Runga–Kutta technique with an adaptive time step. The boundary condition at the center of the microarc was that all spatial derivatives be zero. The boundary condition at the outer parameter of the subvolume in which the microarc equations are being solved is that all of the species' densities be equal to their values in the bulk plasma. This last condition set the maximum radius of the cylindrical mesh used for the microarc, since during the length of the current pulse gas should not convect outside the volume.

For n randomly distributed streamers, the resistance of the discharge is then given by:

$$R_D = \left[\frac{\sigma_b (Lw - n\pi r_{\max}^2)}{d} + \frac{n}{d} \int_0^{r_{\max}} \sigma(r) 2\pi r dr \right]^{-1} \tag{11}$$

where the electrode separation, length, and width are d, L, and w; $\sigma(r)$ is the local conductivity in the subvolume containing the streamer, σ_b is the conductivity in the bulk plasma, and $r_{\max}$ is the maximum extent of the streamer subvolume. To investigate small-scale nonuniformities, we specified that the preionization electron density has the form:

$$n_{e0}(r) = n_{e0} \cdot \left(1 + \alpha \cdot \exp\left(-(r/r_0)^2\right)\right) \tag{12}$$

where n_{e0} is the preionization density in the bulk plasma, α is the magnitude of the inhomogeneity, and r_0 is its spatial extent.

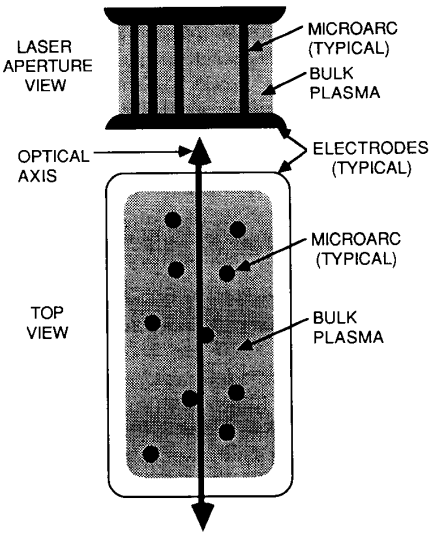

Fig. 2. Schematic of the combined microarc–bulk plasma model for the discharge excimer laser. The microarcs are modeled using the hydrodynamic conservation equations. They are conceptually randomly scattered throughout the discharge volume and obscure laser radiation in the plane of the optical aperture.

The plasma in the microarc is highly excited when the microchannel rarifies and nearly comes into equilibrium with the electron temperature, which may exceed 10 eV. This results in a high density of atomic excited states within a few electronvolts of the ionization limit. Absorption of UV photons by the plasma column can be expected to be high. Large changes in the index of refraction may also have a significant lensing effect. In this respect, laser shadowgraphs and interferograms of laser-triggered spark graphs through gas mixtures having large mole fractions of high atomic weight constituents have been made using KrF illumination [32]. These measurements showed many of the columns to be nearly black. Optical imaging was required to compensate for the lensing effect of the cylindrical column. Since the microarcs in KrF laser discharges have similar properties, they too should shadow the laser radiation in the direction of propagation. As a worst-case analysis, we made this assumption in the model. After a fairly comprehensive parameterization of the model, we found that formation of a microarc occurs rapidly after the channel rarifies by ≈ 0.15 of its initial density. The diameter of a microarc which obscures laser radiation was, therefore, taken as that value when the fractional rarification is 0.15. The laser output power was then reduced by the fractional cross-sectional area of the output plane that was obscured by the microarcs having at least this value of rarification.

The experimental conditions for this study are those of Watanabe and Endoh [4]. The device uses a $He/Kr/F_2 = 99.47/0.44/0.09$ gas mixture at 4.5 atm. The active volume of the discharge is $7 \times 7 \times 80$ cm^3. An intrinsic laser-energy efficiency of 1.2%

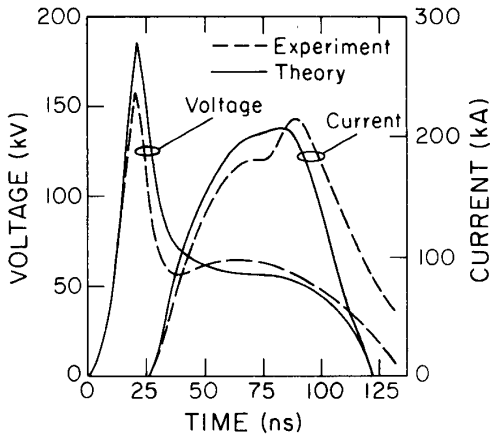

Fig. 3. Theoretical and experimental [4] current and voltage waveforms of a large aperture KrF(B → X) laser.

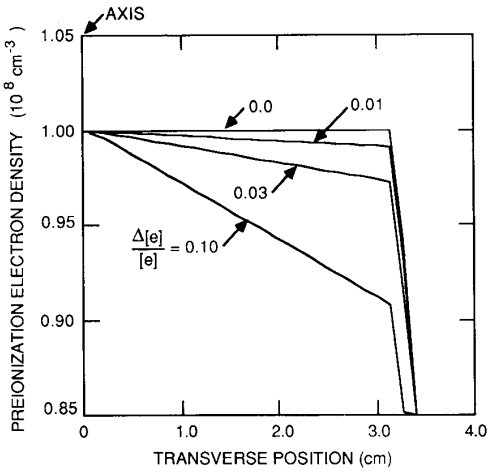

Fig. 4. Preionization electron density profiles for our parametric study. The discharge is symmetric across the center line. The dimension shown is parallel to the electrodes and perpendicular to the optical axis.

was obtained with an output energy of 10 J. A comparison of experimental and theoretical waveforms is shown in Fig. 3. The predicted laser efficiency is 1.4%. When including microarcs in the calculation, the experimental conditions of Watanabe and Endoh [4] were also used, except that the PFL was lengthened to 200 ns.

IV. Simulation of Electric-Discharge-Excited KrF Lasers with Nonuniformities

In this section we discuss the consequences of large-scale and small-scale nonuniformities on the performance of electric-discharge-excited KrF lasers. We will first discuss the consequences of large-scale nonuniformities that result in macroscopic arcing. We then examine small scale nonuniformities which are the precursors to microarcs.

A. Large Spatial Scale Nonuniformities

The OPI results from a nonuniformity in the electric field, preionization electron density, or gas mixture which results in inhomogeneous burnup of the halogen donor. The consequences of macroscopic nonuniformities in these parameters have been previously investigated in electric-discharge-excited HgBr lasers [30]. Since the trends are similar in KrF lasers, we will only briefly address this spatial scale. The most common source of nonuniformity is the preionization electron density. To investigate this effect, the preionization density profile in a discharge KrF laser was varied, as shown in Fig. 4 with a maximum value of 10^8 cm^{-3}. The following results in this section are insensitive to the value of n_{e0} over the range of $< 10^8$ cm^{-3} to $> 10^{10}$ cm^{-3} other than for the duration of the avalanche. The impact of the value of n_{e0} on laser performance is discussed in Section IV-C. The spatial dimension in the figure is parallel to the electrodes and perpendicular to the optical axis. Power deposition as a function of time and position between the electrodes is shown in Fig. 5(a) for an edge-to-center fractional nonuniformity in n_{e0} of 0.1. The fractional misalignment in the electrodes is 0.001 (see below). In this and all cases, power deposition at the leading edge of the discharge pulse is fairly uniform as a function of position, and no less uniform than the preionization density. At these early times, the F_2 has not been significantly depleted so that all spatial locations have nearly the same operating point $[(E/N)_s]$. As F_2 begins to become depleted more rapidly near the axis where the preionization density is the highest, the stable operating point at those locations decreases to a value smaller than the average E/N across the gap. The result is an ionization excess which initiates an electron avalanche, resulting in more rapid depletion of F_2 and causing constriction of the discharge. The F_2 density and power deposition as a function of position for the conditions of Fig. 4 are shown in Fig. 6. The time is 150 ns after triggering. The increase in local power deposition strongly correlates with the depletion of F_2. Even though the depletion of F_2 and power deposition are strong functions of position, the total power deposition in the discharge does not dramatically change. This topic is further discussed below.

Departures from the operating point can be initiated by changes in the mole fraction of species, as discussed above, or may be ingrained in the system due to nonuniformities in E/N due to misaligned electrodes [33] and imperfections on the surface of the electrodes [34]. The former leads directly to an OPI, because $(E/N)_s$ cannot be simultaneously provided at all points. There are, then, rapid changes in the halogen mole fraction resulting from the different degrees of ionization excess provided by different E/N. As Osborne [33] points out, the ionization excess which results from changing E/N from the operating point is a sensitive function of gas mixture, tending to be worse for fluorine mixtures (e.g., He/Kr/F_2) than for chlorine mixtures (e.g., He/Xe/HCl), and may explain the shorter pulse lengths obtained in fluorine mixtures.

To investigate the sensitivity of the OPI to nonuniformities in E/N caused by misalignments of the electrodes, a linear edge-to-center variation in E/N was specified in the model. The E/N was highest on the axis. Power deposition as a function of position and time for a 0.01 edge-to-center variation is plotted in Fig. 5(b). The nonuniformity in preionization density is 0.1, which is common for spark array preionization [35]. The F_2 density and power deposition as a function of position for electrode misalignments of 0.001, 0.003, and 0.01 are shown in Fig. 7. The time is 150 ns after triggering. The constriction of the discharge occurs almost immediately for a misalignment of 0.01, resulting in virtually total depletion of F_2 on the axis, as shown in Fig. 7(a). The sensitivity of discharge constriction to

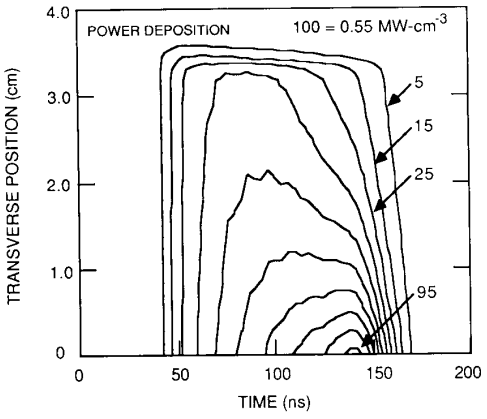

(a)

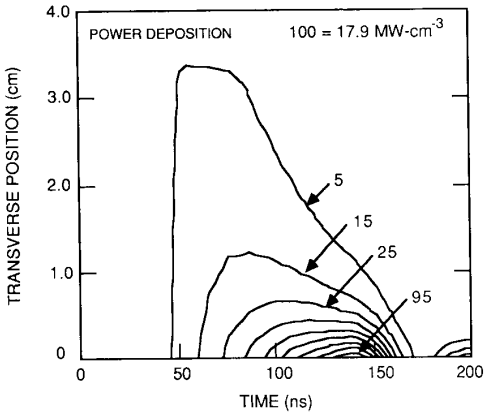

(b)

Fig. 5. Power deposition as a function of position and time in the electric discharge KrF laser. The discharge is symmetric across the center line. The dimension shown is parallel to the electrodes and perpendicular to the optical axis. (a) Power deposition for a 0.1 nonuniformity in preionization density. (b) Power deposition for a 0.01 edge-to-center misalignment of the electrodes resulting in a commensurate edge-to-center variation in electric field.

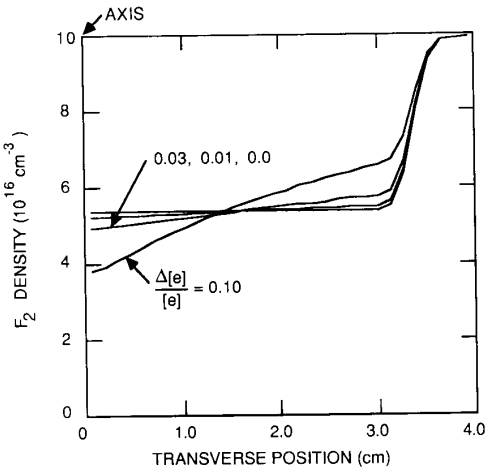

(a)

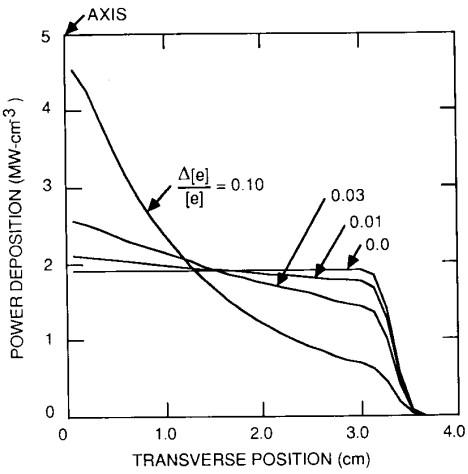

(b)

Fig. 6. Density of (a) F_2, and (b) power deposition at t = 150 ns as a function of position for the preionization electron density profiles shown in Fig. 4. More uniform preionization results in more severe constriction.

misalignments in the electrodes is quite high, with significant constriction occurring by the end of the pulse with only a 0.001 misalignment. There appears, though, to be a threshold for obtaining arc-like conditions of between 0.003 and 0.01 misalignment, as shown by the profiles for power deposition in Fig. 7(b).

Total discharge power deposition and laser power are plotted as a function of time for various electrode misalignments in Fig. 8. Although there is severe constriction of the discharge, total power deposition is not adversely affected. This results from the fact that the current delivered to the discharge is ultimately limited by the impedance of the PFL. The constrictions resulting from nonuniform power deposition on these spatial scales are therefore not accurately described as arcs, since there is no rarification and the current is externally limited. The total laser power, though, is a more sensitive function of constriction of the discharge, as shown in Fig. 8(b). The more constricted cases result in lower total laser power. The decrease in laser power is due to a higher rate of electron collision quenching of KrF(B) and a reduction in the efficiency of the harpooning reaction [36] (i.e., $Kr^* + F_2 \rightarrow KrF(B) + F$) due to depletion of F_2 in the constricted regions.

The fact that laser pulses can be quite long (100–150 ns) in spite of there being severe macroscopic spatial nonuniformities in power deposition, motivates one to examine other causes for termination of the laser pulse. In the next subsection we examine small-scale inhomogeneities as a possible cause.

B. Small Spatial Scale Nonuniformities

The validity of the SKA for modeling high-pressure pulsed gas discharges depends upon the spatial scale of nonuniformities in the electric field, preionization electron density, or gas mole fractions, and the duration of the discharge pulse. These parameters determine whether significant convection will occur, which would lead to further changes in E/N and eventually to instabilities. In this subsection we will investigate this spatial scale by modeling the formations of microarcs in electric discharge excimer lasers.

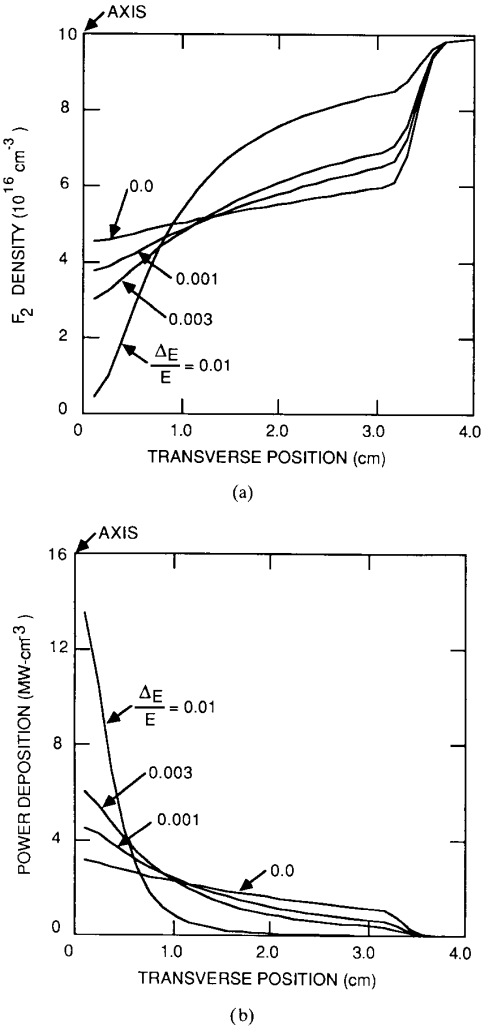

Fig. 7. Density of (a) F_2, and (b) power deposition as a function of position for edge-to-center misalignments of the electrodes of 0.001, 0.003, and 0.01. The misalignments result in edge-to-center variations in the electric field. Only nominal misalignments result in rapid constriction.

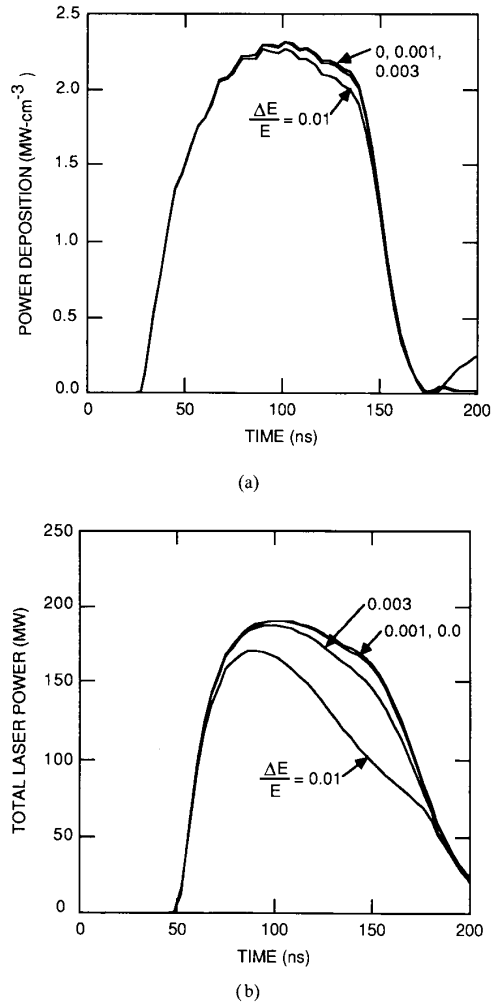

Fig. 8. Total (a) power deposition, and (b) laser power as a function of time for different edge-to-center misalignments of the electrodes indicated by the resulting variation of the electric field. Laser power is more sensitive to constriction than power deposition due to the depletion of F_2.

A recurring trend we will encounter is that if the size of a nonuniformity r_0 is small enough and its magnitude α is large enough, rarification and arcing occur. If a microarc succeeds in developing, those having a larger value of r_0 have a more detrimental effect on laser performance, because they subtend a larger cross-sectional area and therefore optically spoil more of the laser. For a given value of α, one therefore would like to have one of two conditions: One would like as small a value of r_0 as possible so that even though microarcs may form, a large number will be required to spoil the optical homogeneity of the discharge and obscure the laser flux. Alternatively, for a given value of α and number of nonuniformities, one would like r_0 to be as large as possible so that microarcs will not develop during the time of interest. In any case, the best strategy is to have α be sufficiently small so that microarcs do not develop.

Using the microarc-bulk plasma model, preionization density was selected as the source of nonuniformity, and (11) was used for n_{e0} in the vicinity of the inhomogeneity. The bulk value of the preionization electron density was 10^9 cm^{-3}. The total gas density and F_2 density in the vicinity of the nonuniformity ($\alpha = 0.05$, $r_0 = 20$ μm) as calculated with the model are plotted in Fig. 9. The voltage is switched onto the head at $t = 0$ and the duration of the avalanche is $\approx$ 50 ns, at which time the current begins to rise (see Fig. 3). Note that the F_2 density outside the core uniformly decreases due to the normal progression of burnup. The rarification of F_2 in the core is more severe than that of the bulk due to the higher rate of burnup resulting from dissociative electron attachment, direct dissociation by electron impact, and harpooning reactions in the core of the nonuniformity. There is only nominal gas motion for $t < 100$ ns. As F_2 is depleted and the local power deposition in the core increases, though, advection begins. The combined effects of rarification and depletion of F_2 result in a decrease in the local operating point (that is, a decrease in $(E/N)_s$) and a strong ionization excess in the core. Even at this early time, there is nearly an order of magnitude increase in the electron density and

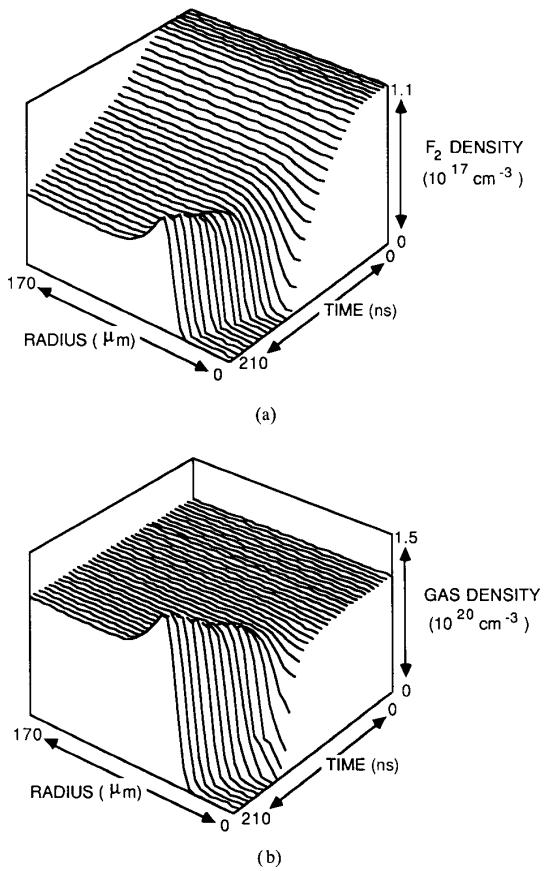

Fig. 9. F_2 density (top) and gas density (bottom) as a function of radius and time in the vicinity of a microarc showing the onset of rarification. F_2 is uniformly depleted outside the core as part of the normal burnup which occurs during operation of the laser.

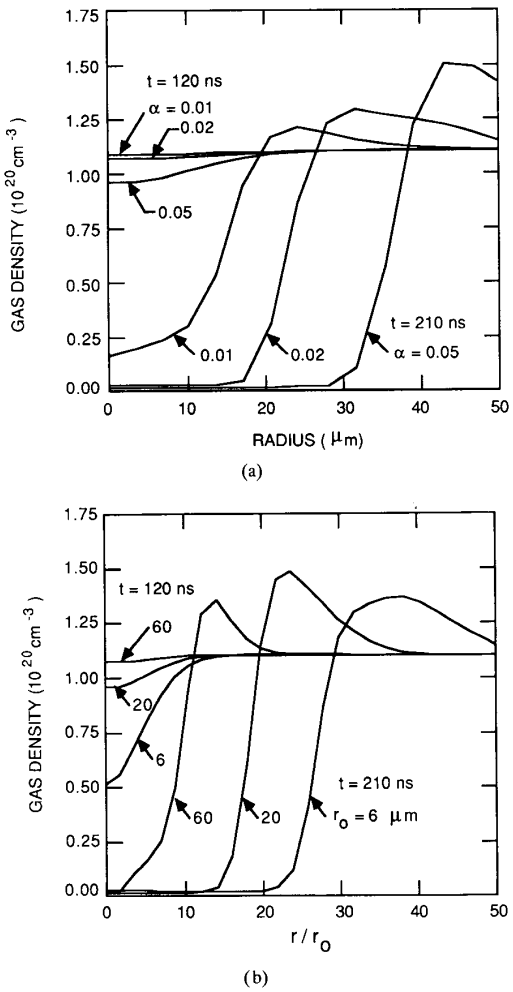

Fig. 10. Gas density as a function of radius at t = 120 ns and 210 ns for different (a) degrees of nonuniformity α in the preionization electron density, and (b) extent of the nonuniformity r_0. In the lower figure, the radius has been normalized by r_0. Rarification occurs earlier with larger values of α and smaller values of r_0. The absolute extent of the microarc, though, may be larger with large values of r_0.

power deposition in the core of the developing microarc. The higher power deposition in the core causes a substantial increase in the gas temperature. It is this increase in gas temperature and the small scale of the nonuniformity which set up a large enough pressure gradient to drive radial advection. As we will discuss below, the contribution of the microarcs to the total conductivity of the discharge is, at this time, small. Therefore the applied electric field does not change, remaining the value determined by the conductivity of the bulk plasma. This value is greater than $(E/N)_s$ in the core. The rarification of the core is clearly unstable due to the decrease in its operating point below that of the average E/N of the discharge. The result is a true microarc, generating a "blast" or rarification wave from the core as shown in Fig. 9. The small oscillations in the radius of the core result, in part, from oscillations in the current.

To investigate the propensity of forming microarcs the spatial extent of the nonuniformity was parameterized using 6 μm < r_0 < 60 μm, and the degree of the nonuniformity was parameterized using 0.01 < α < 0.05. The gas density in the vicinity of the nonuniformity at 120 and 210 ns is shown in Fig. 10. (See Fig. 9 for relative timing.) The spatial coordinate has been normalized by r_0 in Fig. 10(b). When r_0 is constant, in this case at 20 μm, the onset of the microarc occurs earlier and is more severe when α is larger, as shown in Fig. 10(a). At t = 120 ns, which corresponds to the peak of the current pulse, there has been no rarification for $\alpha \leq 0.02$, whereas the microarc has already begun to form for $\alpha = 0.05$. By 210 ns the microarc has fully developed for $\alpha \geq 0.01$. The radii of the channels at this time increase with increasing α, a result of the shorter incubation time when α is larger. In Fig. 10(b) we kept $\alpha = 0.05$ and varied r_0. The microarcs start at earlier times when r_0 is smaller, since, for a given α, the pressure gradient and hence initializing force for advection is larger with the smaller spatial scale. The *normalized* radius of the microarc channel r/r_0 is larger with smaller values of r_0 due to the shorter incubation time. Note, however, that once the microarc develops, the *absolute* width of the channel may be larger with larger values of r_0.

The results in Fig. 10 confirm the scaling relationship of (4) that states that microarcs form more rapidly with smaller values of r_0 and larger values of α. Once a microarc develops, though, its severity increases with increasing r_0. For a given duration of

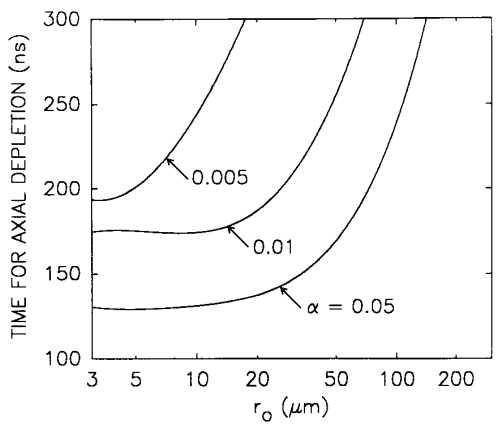

Fig. 11. The time required to rarify gas on the axis of a developing microarc as a function of r_0 for different degrees of nonuniformity α in preionization density. The incubation time for rarifying the channel increases with decreasing α and increasing r_0.

current flow there are values of r_0 and α for which rarification of the channel will not occur and for which microarcs will not form. These values are shown in Fig. 11, where the time required to rarify the channel on the axis of the microarc is shown as a function of r_0 for different values of α. This time increases with decreasing α and increasing r_0. A rough scaling law can be obtained by noting that the values of r_0 and α for which rarification occurs at 250 ns obey $\frac{r_0}{\alpha^{1/2}} \approx 150$ μm.

The effect of microarcs on the impedence of the discharge depends on the proportion of current carried by the streamers relative to the bulk homogeneous plasma, since the electric field is the same for both. The microarcs appear to be parallel resistors to the bulk plasma and the current is divided accordingly. In this respect, the impact of the microarcs is determined by both the amount of current each arc carries and the area density δ (number/electrode area) of the microarcs. The effect that microarcs have on laser performance is therefore two-fold: First, power which is dissipated in the microarcs is not channeled to the upper laser level in a useful fashion and is therefore wasted. Second, the optical homogeneity of the gas is spoiled by microarcs which, in our approximation, shadow the laser radiation. In both respects the area density of the microarcs is an important consideration. This value depends on many system parameters (e.g., condition of the surface of the electrodes, uniformity of the spark arrays, or the X-ray windows) whose simulation is beyond the scope of this work. Based on experimental observations [15], [28] and parameterization of the model, however, we can estimate the value of δ for typical conditions. This was done by noting that the optical pulse length of KrF lasers rarely exceeds 150 ns, and that microarcs are initially < 10's–100 μm in size. As a result of this parameterization we found that for select conditions the optical pulse terminated at 150 ns for $\delta \approx 1.5$–2.0 cm^{-2}.

Laser power, total bulk discharge power, and the fractional amount of discharge power dissipated in the microarcs are plotted in Fig. 12 for $\alpha = 0.05$ and different r_0. The streamer density is approximately $\delta = 1.7$ cm^{-2}. Although the total bulk discharge power decreases slightly with increasing r_0, only a small fraction of the power is dissipated in the microarcs until their cores rarify and F_2 is depleted. At this time their expansion is rapid and the current is quickly channeled through them. For our conditions this occurs at 150–200 ns, or 100–150 ns after avalanche. The optical homogeneity of the laser, though, has been significantly spoiled prior to this time. Total laser power decreases and eventually ceases, for this reason, prior to discharge power being siphoned away by the microarcs. In the worst case, the laser pulse is terminated with only 8% of the discharge power being dissipated in the microarcs. These results are in qualitative agreement with the experimental observations of Taylor [15] and Osborne and Hutchinson [28]. In both cases, laser power was observed to terminate coincidently to the development of microarcs. At this time, however, power continued to be fairly uniformly deposited in the discharge, as confirmed by sidelight fluorescence and a steady current-voltage characteristic.

The results in Fig. 12 show that laser power begins to decrease earlier, and power is channeled to the microarcs earlier, when r_0 is small. This trend is due to the shorter incubation time required to rarify the core for smaller values of r_0. (For these conditions, nonuniformities having $r_0 > 70$–80 μm do not create microarcs for $t < 200$ ns.) Even though they start sooner, microarcs starting with small values of r_0 have small radii and therefore obscure only a small fraction of the laser flux. Microarcs starting with large values of r_0 take longer to form. Once they form, however, they are more detrimental to laser performance, since with their larger cross-sectional area they obscure a larger fraction of the laser flux. The general scaling is then that α should be small and r_0 large to prevent microarcs from forming. If, however, microarcs form then for a given value of δ, then arcs beginning with a larger value of r_0 are more detrimental to laser performance.

One might expect from statistical arguments that the area density of the nonuniformities having small values of r_0 is larger than those having large values of r_0. In this respect the area density of microarcs δ which limit the optical pulse to a total length of 150 ns is plotted in Fig. 13 for the same parameters as in Fig. 11. A higher area density of microarcs is generally required to terminate the optical pulse with smaller values of α and larger values of r_0. If, however, r_0 is large enough, then microarcs do not form and the laser pulse is not prematurely terminated. The upturn in δ for $\alpha = 0.005$ is a consequence of the microarcs not fully developing during the time of interest. Therefore more arcs are required to terminate the laser pulse.

C. Scaling with Electron Density

In the previous discussion the source of the inhomogeneities was not addressed. We have also not addressed the dependence of laser pulse length on the preionization density n_{e0}. It has been observed by many workers that laser power and pulse length increase with increasing preionization density [15], [37]. There is, however, no physical mechanism in the conventional understanding of the volume-averaged plasma kinetics which demands such a scaling. In fact, parameterizing models of electric-discharge excimer lasers that only consider volume-averaged kinetics as a function of n_{e0} over a large range (10^7–10^{11} cm^{-3}) yields only a nominal effect on laser pulse length. This directly conflicts with experiments. We suggest that the source of inhomogeneities in n_{e0} and the dependence of laser performance on preionization density may, in fact, result from the same phenomena.

To explore this issue, consider a volume of gas having radius r_0 and length $\ell = v_d \cdot \Delta t$, where v_d is the drift velocity of electrons during the avalanche stage, and Δt is the avalanche time. The total number of preionization electrons in this volume is simply $N = \pi r_0^2 \ell n_{e0}$. If we equate the nonuniformity factor α with the

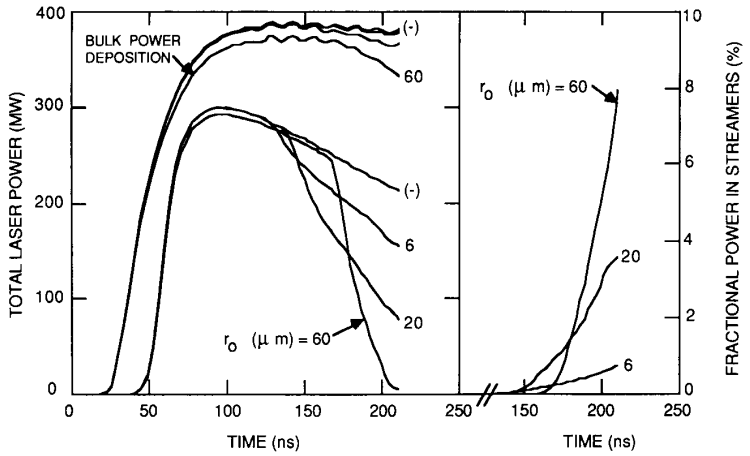

Fig. 12. Laser power, total bulk discharge power, and fraction of the discharge power dissipated in the microarcs as a function of time for different values of r_0. (The notation (−) signifies there being no microarcs.) The degree of nonuniformity is $\alpha = 0.05$ and the area density of microarcs is $\delta = 1.7\ \text{cm}^{-2}$. Microarcs with large values of r_0 take longer to develop, but are ultimately more detrimental to laser performance. For these conditions, microarcs do not form for $t < 200$ ns if $r_0 > 70$–$80\ \mu$m.

random fluctuations of n_{e0} in this volume, then:

$$\alpha = \frac{N^{1/2}}{N} = \frac{1}{r_0(\pi n_{e0} v_d \Delta t)^{1/2}} = \frac{0.8}{r_0(\mu m)\,(n_{e0}(10^9\ \text{cm}^{-3}))^{1/2}}. \tag{13}$$

On the right-hand side of (12), $v_d = 10^6\ \text{cm-s}^{-1}$ and $\Delta t = 50$ ns have been taken as typical values. Units of micrometers and $10^9\ \text{cm}^{-3}$ have been used for r_0 and n_{e0}.[1] Using (12), the preionization density and r_0 which result in a given value of α are shown in Fig. 14. Statistically, smaller values of α are obtained with larger values of r_0 and larger values of n_{e0}. For example, to insure that microarcs do not quickly form, we need to keep $\alpha < 0.1$ and $r_0 \geq 10\ \mu$m. These parameters require that $n_{e0} \geq 10^9\ \text{cm}^{-3}$, which is commensurate with the preionization density above which the laser energy is nearly constant [15]. Conversely, the characteristic radius for which a statistical nonuniformity of $\alpha = 0.1$ is obtained at a preionization density of $n_{e0} = 10^8\ \text{cm}^{-3}$ is 25 μm.

We see then, that even though n_{e0} has virtually no effect on laser pulse length based on volumetrically averaged kinetics, the statistical variation of electron density in small volumes caused by small n_{e0} can result in values of α which generate microarcs. The microarcs are then the disrupting mechanism for the laser pulse. The propensity to form microarcs decreases with larger values of n_{e0}, which then results in longer optical pulse lengths. Based on these arguments the critical values of n_{e0} are 10^8–$10^9\ \text{cm}^{-3}$, which are almost two orders of magnitude larger than those stipulated by the Levatter and Lin criterion (Equation (3) and [25]).

D. Dependence of Optical Pulse Length on Halogen Density

It has also been observed that the optical pulse length in electric-discharge-excited excimer lasers increases with the decreasing fraction of the halogen donor (HCl in XeCl lasers and F_2 in KrF lasers) [3], [15], [39], [40]. The pulse length also increases with a decreasing rate coefficient for electron attachment [33]. Based on our discussion in the previous sections, one might attribute this behavior to the fact that lower halogen densities result in higher preionization densities, which statistically result in nonuniformities which have larger values of r_0 and smaller values of α. Using a nonstatistical argument, however, one may also attribute this behavior to nonuniformities in the source of preionization electrons which are more readily homogenized at lower halogen densities. This latter scaling may be derived by examining the preionization phase of the discharge. The preionizing X-ray or UV radiation pulse is usually applied prior to there being significant voltage across the discharge electrodes

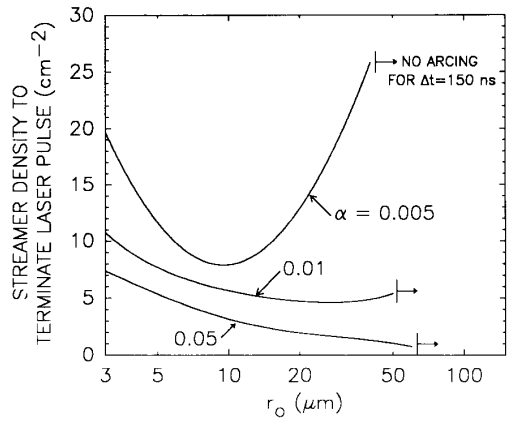

Fig. 13. The area density of microarcs δ (cm^{-2}) required to limit the laser pulse to 150 ns as a function of r_0 for different degrees of nonuniformity in preionization density α. The required area density increases with decreasing α and decreases with increasing r_0. If, however, r_0 is large enough, microarcing will not occur. The upturn in δ for $\alpha = 0.005$ is a consequence of the microarcs not fully developing during the time of interest. Therefore more arcs are required to terminate the laser pulse.

[1] A similar statistical relationship between preionization density and laser performance was presented by Letardi *et al.* simultaneous to this submission (see reference [38]).

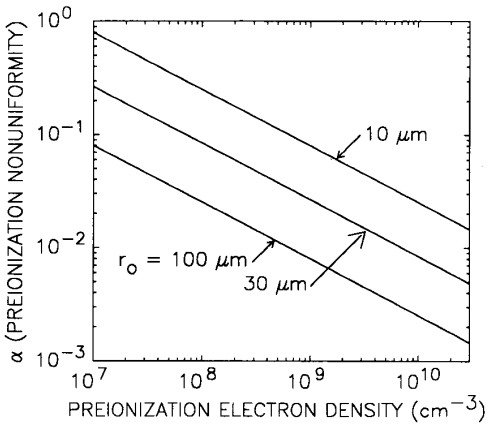

Fig. 14. Nonuniformity in preionization electron density α as a function of n_{e0} and r_0. These values are based on statistical fluctuations of electrons in the small volume defined by r_0.

[9]. Under these conditions the preionization electron density n_{e0} is approximately given by:

$$\frac{\partial n_{e0}(\vec{r}, t)}{\partial t} = S(\vec{r}) - Dv^2 n_{e0} - n_{e0} k_a M \simeq 0 \qquad (14)$$

where S is the source function for preionization (cm^{-3} s^{-1}), D is the electron diffusion coefficient (cm^2 s^{-1}), and k_a is the rate coefficient for electron attachment (cm^3 s^{-1}) to the halogen donor having density M (cm^{-3}). If the halogen density is sufficiently high so that the mean-free path for attachment is much shorter than the diffusion length, then:

$$n_{e0}(\vec{r}) \simeq \frac{S(\vec{r})}{k_a M(\vec{r})}. \qquad (15)$$

For these conditions any nonuniformities in either the source function or halogen density are "frozen" into the preionization density profile. If, however, the halogen density is sufficiently low so that the diffusion length exceeds the mean-free path for attachment, then any nonuniformities in either $S(\vec{r})$ or $M(\vec{r})$ are homogenized by electron diffusion. Therefore, given that the scale length of the nonuniformity in the source function or halogen density is r_0, the preionization density will be spatially uniform if:

$$M \ll \frac{D}{r_0^2 k_a}. \qquad (16)$$

To demonstrate this scaling the preionization density $n_{e0}(r)$ was obtained from (13) using different values of k_a. The preionization source $S(r)$ has a nonuniformity of magnitude, α = 0.05, with the shape given by (11) (r_0 = 10 μm). The results for $n_{e0}(r)$ are shown in Fig. 15(a) using $0.1 \cdot k_0 < k_a < 10 \cdot k_0$ for $k_0 = 3 \times 10^{-9}$ cm^3 s^{-1}. (The effect scales with $k_a \cdot M$.) The cases with the smaller values of $k_a \cdot M$ result in a more uniform preionization density. When these preionization profiles are used as initial conditions in the model, the onset of microarcs occurs later with the more uniform profiles (that is, small smaller values of $k_a \cdot M$), as shown in Fig. 15(b). To eliminate other effects, only the preionization profiles differ in these three cases. Lower halogen densities, or more specifically, smaller values of $k_a \cdot M$, may then result in longer optical pulse lengths due to the more uniform preionization which can be obtained when

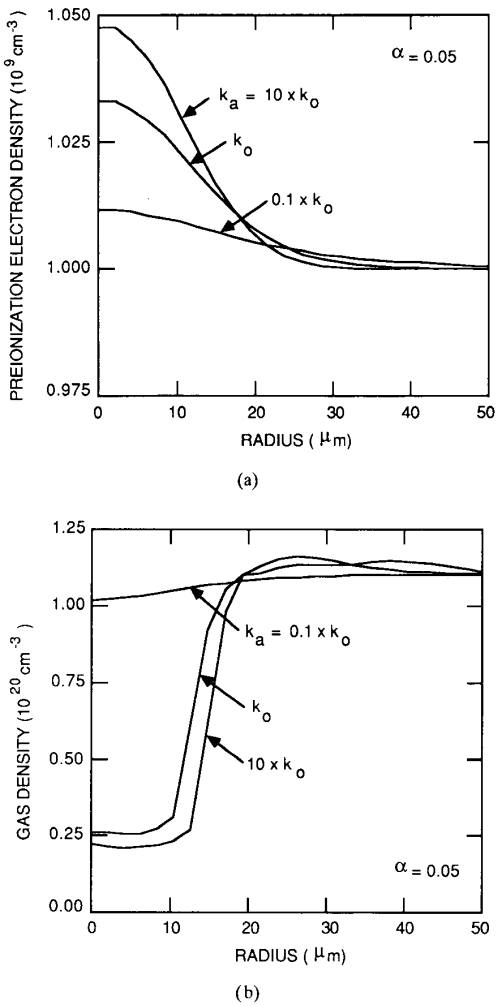

Fig. 15. Discharge parameters for different values of the rate coefficient for dissociative attachment to F_2 during the preionization phase. (a) Preionization electron density. (b) Gas density at t = 150 ns. The cases with larger values of $k_a \cdot M$ form microarcs at earlier times.

the homogenizing effects of diffusion during the pre-avalanche period are important. This effect is independent of the statistically smaller values of α which are obtained with smaller values of $k_a \cdot M$, and hence larger n_{e0}.

These results may help to explain why optical pulses are generally shorter in KrF lasers using F_2 as the halogen donor compared to XeCl lasers using HCl as the halogen donor. The dissociative attachment cross section is a function of the vibrational state of both of these molecules [41]. In HCl, the dissociative cross section is small for v= 0 (10^{-17} cm^2) and has a high threshold energy (0.75 eV). The cross section increases to 10^{-14} cm^2, and the threshold energy decreases to nearly zero for v= 3. In F_2, the cross section is $\simeq 5 \times 10^{-16}$ cm^2 for v= 0, decreases with increasing vibrational level, and is finite at nearly zero electron energy. During the preionization and avalanche phase the current density is low and the fraction of HCl and F_2 molecules which are vibrationally excited is negligibly small. Therefore with equal mole fractions of the halogen donor, the rate of attachment in F_2 mixtures is more than an order of magnitude

larger than in HCl mixtures. This results in smaller values of n_{e0} and conditions which "freeze" any nonuniformities in halogen density or the preionization source in F_2 mixtures. Both of these conditions more readily result in microarcs which can reduce the length of the laser pulse.

V. Concluding Remarks

The effects of large scale and small-scale nonuniformities on the performance of electric-discharge-excited KrF lasers has been theoretically studied. The relationship between the development of microarcs and the length of the optical pulse was investigated. We found that the optical pulse in lasers having microarcs with a density of $> 1-2\ \mathrm{cm}^{-2}$ terminated prior to the collapse of the impedance of the discharge due to disruption of the optical homogeneity of the discharge. These results parallel those observed experimentally. The observation that laser pulse lengths increase with decreasing halogen density can be explained by the statistical nonuniformity of preionization density in small volumes or the ability of diffusion by electrons to homogenize nonuniformities in preionization or halogen density. High halogen densities cause the preionization density to more closely align with inhomogeneities in the source or halogen density, thereby providing the initial conditions for microarcs to form.

Acknowledgment

The author would like to thank Dr. R. S. Taylor for motivating this study and for his helpful comments, Dr. C. Fisher for his experimental expertise and tutelage in developing long pulse excimer lasers, and Dr. M. Osborne for providing preprints of his works. The author would also like to thank Prof. J. T. Verdeyen for pointing out the statistical variation of preionization density.

References

[1] Ch. A. Brau, in *Excimer Lasers,* Ch. K. Rhodes, Ed. Berlin: Springer-Verlag, 1979, pp. 87–134.
[2] F. Kannari, M. Obara, and T. Fujioka, "An advanced kinetic model of electron-beam-excited KrF lasers including the vibrational relaxation in KrF*(B) and collisional mixing of KrF*(B, C)," *J. Appl. Phys.,* vol. 57, pp. 4309–4322, 1985.
[3] R. S. Taylor and K. E. Leopold, "Ultralong optical-pulse corona preionized XeCl laser," *J. Appl. Phys.,* vol. 65, pp. 22–29, 1989.
[4] S. Watanabe and A. Endoh, "Wide aperture self-sustained discharge KrF and XeCl lasers," *Appl. Phys. Lett.,* vol. 41, pp. 799–801, 1982.
[5] G. J. Hirst, V. Rivano, and C. E. Webb, "Spatially resolved gain measurements in a discharge-pumped KrF laser amplifier," *J. Appl. Phys.,* vol. 61, pp. 2438–2444, 1987.
[6] T. Hasama, K. Miyazaki, K. Yamada, and T. Sato, "50-J discharge pumped XeCl laser," *IEEE J. Quantum Electron.,* vol. 25, pp. 113–120, 1989.
[7] L. G. Champagne, A. J. Dudas, and N. W. Harris, "Current Rise-time limitations of the large volume X-ray preionized discharge-pumped XeCl laser," *J. Appl. Phys.,* vol. 62, pp. 1576–1584, 1987.
[8] U. Schmidt and W. Rath, "High average power laser development in Europe," in *Summary 1990 Conf. Lasers and Electro-optics* (Anaheim, CA), 1990, p. 348.
[9] C. H. Fisher *et al.,* "High efficiency XeCl laser excitation with magnetic switching," *Appl. Phys. Lett.,* vol. 48, pp. 1574–1576, 1986.
[10] "Guide to excimer lasers," Photonics Spectra, May 1989, pp. 165–176.
[11] W. H. Long, M. J. Plummer, and E. A. Stappaerts, "Efficient discharge pumping of an XeCl laser using a high-voltage prepulse," *Appl. Phys. Lett.,* vol. 43, pp. 735–738, 1983.
[12] R. S. Taylor and K. Leopold, "Microsecond duration optical pulses from a UV-preionized XeCl laser," *Appl. Phys. Lett.,* vol. 47, pp. 81–83, 1985.
[13] Th. Hammer and W. Botticher, "Spectroscopic investigation of the ionization kinetics in XeCl laser discharges by Xe* density measurements," *Appl. Phys. B,* vol. 48, pp. 73–84, 1989.
[14] A. B. Treshchalov and V. E. Peet, "Spatial-time dynamics of the discharge pumping and lasing in a XeCl laser," *IEEE J. Quantum Electron.,* vol. 24, pp. 169–176, 1988.
[15] R. S. Taylor, "Preionization and discharge stability of long optical pulse duration UV-preionized XeCl lasers," *Appl. Phys. B,* vol. 41, pp. 1–24, 1986.
[16] W. J. Witteman and B. M. H. H. Kleikamp, "On the electron beam-pumped KrF lasers," *J. Appl. Phys.,* vol. 55, pp. 1299–1307, 1984.
[17] S. Suminda, K. Kunitomo, M. Kaburagi, M. Obara, and T. Fujioka, "Effect of preionization uniformity on a KrF laser," *J. Appl. Phys.,* vol. 52, pp. 2682–2686, 1981.
[18] S. Watanabe, A. J. Alcock, K. E. Leopold, and R. S. Taylor, "Spatially resolved gain measurements in UV preionized homogeneous discharge XeCl and KrF lasers," *Appl. Phys. Lett.,* vol. 38, pp. 3–6, 1981.
[19] V. Yu. Baranov, V. M. Borisov, D. N. Molchanov, V. P. Novikov, and O. B. Khristoforov, "Wide-aperture electric-discharge XeCl laser with ultraviolet preionization and 20-J output energy," *Sov. J. Quantum Electron.,* vol. 17, pp. 978–983, 1987.
[20] C. Gorse, M. Capitelli, and M. Dipace, "Time-dependent Boltzmann equation in a self-sustained discharge XeCl laser: Influence of electron–electron collisions and superelastic collisions," *J. Appl. Phys.,* vol. 67, pp. 1118–1120, 1990.
[21] K. Midorikawa, M. Obara, and T. Fujioka, "X-ray preionization of rare gas–halide lasers," *IEEE J. Quantum Electron.,* vol. QE-20, pp. 198–205, 1984.
[22] M. R. Osborne, "Preionization electron density and ion decay measurements in an X-ray preionized rare gas fluoride laser," *J. Appl. Phys.,* vol. 63, pp. 32–37, 1988.
[23] T. S. Fahlen, "Efficient quarter-joule KrF laser with corona preionization," *IEEE J. Quantum Electron.,* vol. QE-15, pp. 311–313, 1979.
[24] R. A. Haas, *Gas Lasers,* vol. 3 in *Applied Atomic Collisions Physics,* E. W. McDaniel and W. L. Nighan, Eds. New York: Academic, 1982, pp. 423–452.
[25] J. I. Levatter and S.-C. Lin, "Necessary conditions for the homogeneous formation of pulsed avalanche discharges at high pressures," *J. Appl. Phys.,* vol. 51, pp. 210–222, 1980.
[26] J. Coutts and C. E. Webb, "Stability of transverse self-sustained discharge-excited long-pulse XeCl lasers," *J. Appl. Phys.,* vol. 59, pp. 704–710, 1986.
[27] J. Coutts, "The halogen donor depletion instability-current pulse-shape effects," *J. Phys. D,* vol. 21, pp. 255–59, 1988.
[28] M. R. Osborne and M. H. R. Hutchinson, "Long pulse operation and premature termination of a high-power discharge-pumped XeCl laser," *J. Appl. Phys.,* vol. 59, pp. 711–715, 1986.
[29] M. J. Kushner and A. L. Pindroh, "Discharge constriction, photodetachment, and ionization instabilities in E-beam sustained discharge excimer lasers," *J. Appl. Phys.,* vol. 60, pp. 904–914, 1986.
[30] M. J. Kushner, A. L. Pindroh, C. H. Fisher, T. A. Znotins, and J. J. Ewing, "Multidimensional modeling of transverse avalanche laser discharges: Applications to the HgBr laser," *J. Appl. Phys.,* vol. 57, pp. 2406–2423, 1985.
[31] M. J. Kushner, "Discharge instabilities initiated by nonuniform laser extraction in E-beam sustained discharge KrF lasers," *J. Appl. Phys.,* vol. 62, pp. 101–107, 1987.
[32] W. D. Kimura, M. J. Kushner, E. A. Crawford, and S. R. Byron, *IEEE Trans. Plasma Sci.,* vol. PS-14, pp. 246–255, 1986.
[33] M. R. Osborne, "Rate-gas–halide discharge stability," *Appl. Phys. B,* vol. 45, pp. 285–291, 1988.
[34] L. J. Denes, L. E. Kline, and R. R. Mitchell, "Arc suppression in excimer laser discharges," in *Proc. Int. Conf. Lasers '81.* McLean, VA: STS Press, 1981, pp. 33–39.
[35] S. Takagi, S. Sato, and T. Goto, "Electron density measurements in UV-preionized XeCl and CO_2 laser gas mixtures," *Japan. J. Appl. Phys.,* vol. 28, pp. 2219–2222, 1989.
[36] J. E. Velazco, J. H. Koltz, and D. W. Setser, "Quenching rate constants for metastable argon, krypton and xenon atoms by fluorine containing molecules and branching ratios for XeF* and

KrF* formation," *J. Chem. Phys.*, vol. 65, pp. 3468–3480, 1976.
[37] S. Sumida, K. Kunitomo, M. Kaburagi, M. Obara, and T. Fujioka, "Effect of preionization on uniformity on a KrF laser," *J. Appl. Phys.*, vol. 52, pp. 2682–2686, 1981.
[38] A similar statistical relationship between preionization density and laser performance was presented by Letardi, *et al.* simultaneous to this submission. T. Letardi *et al.*, "Switchless discharge excimer laser system: Modeling and large volume XeCl laser experiments," in *Summary 1990 Conf. Lasers and Electro-optics* (Anaheim, CA), 1990, pp. 348–349.
[39] D. Lo, "The role of halogen donors in discharge instability of rare-gas halide excimer lasers," *Appl. Phys. B*, vol. 49, pp. 535–540, 1989.
[40] T. Hasma, K. Miyazaki, K. Yamada, and T. Sato, "50 J discharge-pumped XeCl laser," *IEEE J. Quantum Electron.*, vol. 25, pp. 113–119, 1989.
[41] J. N. Bardsley and J. M. Wadehera, "Dissociative attachment in HCl, DCl, and F_2," *J. Chem. Phys.*, vol. 78, pp. 7227–7234, 1981.

Mark J. Kushner (S'74–M'79–SM'89–F'91) was born in Los Angeles, CA, on December 21, 1952. He received the B.A. degree in astronomy and the B.S. degree in engineering from the University of California at Los Angeles in 1976. His M.S. and Ph.D. degrees in applied physics were received from the California Institute of Technology in 1977 and 1979, respectively, where he also held the position of Chaim Weizmann Postdoctoral Research Fellow.

He served on the technical staffs of the Sandia National Laboratory and Lawrence Livermore National Laboratory before joining Spectra Technology, Inc. (formerly Mathematical Sciences Northwest), where he was a Principal Research Scientist and Director of Electron, Atomic, and Molecular Physics. In August 1986 he joined the Department of Electrical and Computer Engineering at the University of Illinois (Urbana–Champaign), where he currently holds the rank of Associate Professor. He has published 70 refereed papers and presented more than 120 conference papers on topics related to gas and solid-state lasers, pulse power plasmas, plasma chemistry, chemical lasers, plasma processing of semiconductors, plasma treatment of toxic gases, and laser spectroscopy.

Dr. Kushner is a member of Phi Beta Kappa, Tau Beta Pi, Sigma Xi, the Optical Society of America, the Materials Research Society, and is a Fellow of the American Physical Society.